We are IntechOpen, the world's leading publisher of Open Access books Built by scientists, for scientists

6,900
Open access books available

185,000
International authors and editors

200M
Downloads

Our authors are among the

154
Countries delivered to

TOP 1%
most cited scientists

12.2%
Contributors from top 500 universities



WEB OF SCIENCE™

Selection of our books indexed in the Book Citation Index in Web of Science™ Core Collection (BKCI)

Interested in publishing with us?
Contact book.department@intechopen.com

Numbers displayed above are based on latest data collected.
For more information visit www.intechopen.com



Chapter

Modal Interferometers Based on a Tapered Special Photonic Crystal Fiber for Highly Sensitive Detection

Vladimir (or Uladzimir) P. Minkovich, Joel Villatoro and Pavel V. Minkovich

Abstract

The use of a tapered special photonic crystal fiber (PCF) with collapsed air holes in the waist (the thinnest part of a taper) for highly sensitive detection of strain, high temperature, and fast detection of hydrogen with concentrations between 1.2 and 5.6 vol.% and biosensing is demonstrated. In the tapered PCF, a fundamental core mode couples to a few modes of the solid taper waist. Owing to the beating between the waist modes, the transmission spectra of the tapered PCF exhibit several interference peaks, which are sensitive to refractive index changes of a medium that surrounds the taper and also to changes of a taper length. The changes can be visualized as a shift of the peaks in the output spectrum pattern.

Keywords: modal interferometer, optical fiber devices, optical fiber sensors, interferometry, photonic crystal fiber

1. Introduction

Photonic crystal fibers (PCFs), also known as microstructured or holey optical fibers [1–4], consist of a waveguiding core surrounded by a system of air channels in glass cladding that run along the length of the fiber and arranged in a hexagonal structure around the core. The structure of PCFs enables new possibilities for optical sensing in comparison with standard optical fibers. The most common approach consists of making a sample to interact with the evanescent fields of the PCF guided modes [5–7]. To do so one has to fill the holes with the sample, a gas or liquid, for example, and then the analysis or detection is carried out. In some situation such a process may be inconvenient or impractical. Mach-Zehnder modal interferometers (MZMIs) based on no adiabatic tapered silica PCFs, first fabricated in our facilities [8–10], are attractive for sensing application because of their intrinsic advantages, such as simplicity of fabrication and practical using, high sensitivity, small size, and immunity to electromagnetic interference and their aptitude for remote measurements. Initially, our MZMIs were used for high-resolution refractive index sensing of liquids with indices ranging from 1.41 to 1.45 [8]. In this work, it is presented

fabrication such MZMIs and also their application for detection (with a very high sensitivity) of strain, high temperature, and fast detection of hydrogen with concentrations between 1.2 and 5.6 vol.% or for biosensing.

2. PCF taper fabrication and operating mechanism

To fabricate tapers we employed a homemade quasi-single-mode large-mode-area PCF consisting of a solid core surrounded by four rings of air holes in a cladding arranged in a hexagonal pattern [11]. A micrograph of a cleaved end face of our PCF before the tapering is shown in **Figure 1** (left). The parameters of our PCF are outer diameter of 125 μm, core diameter of 11 μm, average hole diameter of 2.7 μm, and average hole spacing (pitch) of 5.45 μm. To reduce the PCF diameter, the fiber is heated with an oscillating high-temperature flame torch and slowly stretched ("slow-and-hot" method). A Vytran GPX3400 glass-processing machine also can be used. At such a no adiabatic tapering process, a waist of the PCF (the thinnest part of a taper) can be reduced until the air holes collapse, obtaining a piece of a solid fiber with the diameter $\rho_W \sim$ <33 μm, which can support multiple modes (waist modes). In the first transition zone, see **Figure 1** (right), some energy from the PCF fundamental mode passes to a few waist modes.

The beating of these modes inside the solid waist section is sensitive to an external environment, since the propagation constants of the waist modes depend on it. In the final transition zone, the waist modes are again transformed into the PCF fundamental mode, which intensity is determined by the phase difference between the waist modes [9]. The resulting mode carries the interference information generated at the tapered zone to a detector. If, for the simplicity, we consider only two waist modes for the interference with effective refractive indices n_1 and n_2, then, intensity output is

$$I_t = I_1 + I_2 + 2\sqrt{I_1 I_2}\cos(\Delta\theta), \tag{1}$$

where I_1 and I_2 are the intensities of the interactive waist modes, respectively, and $\Delta\theta$ is the phase difference between them. This phase difference creates the output pattern and depends on the difference between the effective waist mode refractive indices (Δn) and the length of the waist L_0:

$$\Delta\theta = \frac{2\pi}{\lambda}(\Delta n)\, L_0, \tag{2}$$

where λ is the center wavelength of the light source used. The interferometer transmittance maxima will be at $2\pi\Delta nL_0/\lambda = 2\pi m$, where m is an integer. Peaks in the output spectrum pattern will be appeared at wavelengths given by $\lambda_m \approx \Delta nL_0/m$, and the spacing between consecutive peaks (period) is provided by $P \approx \lambda^2/\Delta nL_0$. When the refractive index of the surrounding medium is changed, Δn is changed too (keeping L_0 fixed), and a change of phase is generated. This change can be visualized as a peak shift in the output spectrum pattern. The shift in the output spectrum pattern is also happened, when L_0 is changed [9]. It should be pointed out that additional losses, because of PCF tapering, were found to be typically below 3 dB. To test our sensors, we implemented a simple light transmission measuring setup consisting of a low-power light-emitting diode (LED) with peak emission at 1280 nm (or 1550 nm) and about 40–80 nm of spectral width and an optical spectrum analyzer (OSA), Ando AQ-6315E. The tapered PCFs (with a PCF full length of approximately 30 cm) were fusion spliced between standard fibers (SMF-28), and the tapered section was held straight and secured in a mount in all the experiments.

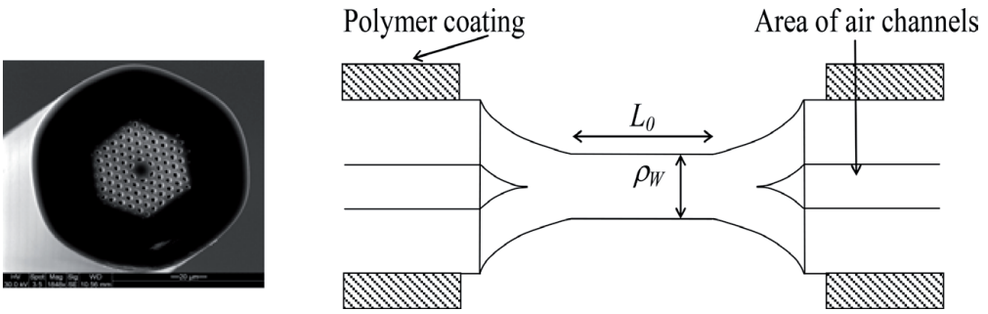


Figure 1.
Image of the cross section of an untapered PCF (left) used to fabricate our tapers and illustration of a uniform-waist tapered PCF (right). L_o *is the length of the uniform waist, and* ρ_W *is the taper waist diameter.*

3. Strain detection

There are a number of applications in which the monitoring of strain-induced changes is important. Some designs based on standard optical fibers have been reported in the literature. For example, strain sensors based on in-fiber gratings [12] and Brillouin scattering [13] are commercially available. The main shortage of these strain sensors is their high thermal sensitivity [14]. In this case, one needs to simultaneously and independently measure strain and temperature [12, 13]. So, the complexity of the sensor is increased. It is necessary to mention that a few attempts to sense strain with PCFs have been reported in the literature at the beginning of our study. They include the use of Brillouin frequency shift [15], long-period grating [16], and fiber Bragg grating [17, 18]. However, these sensors also exhibit an undesirable cross sensitivity to temperature. The application of our tapered PCFs with collapsed air holes for temperature-independent strain sensing is described in this section [19, 20]. Using the fiber, and the tapering process as described in a previous section, a silica PCF taper with waist diameter ρ_W = 28 μm and L_0 = 5 mm was fabricated. **Figure 2** shows the normalized transmission spectra of the used PCF before (dotted line) and after (continuous line) a no adiabatic tapering process.

The measurements were carried out in a measuring setup consisting of an LED, with peak emission at 1540 and 40 nm of spectral width, and an optical spectrum

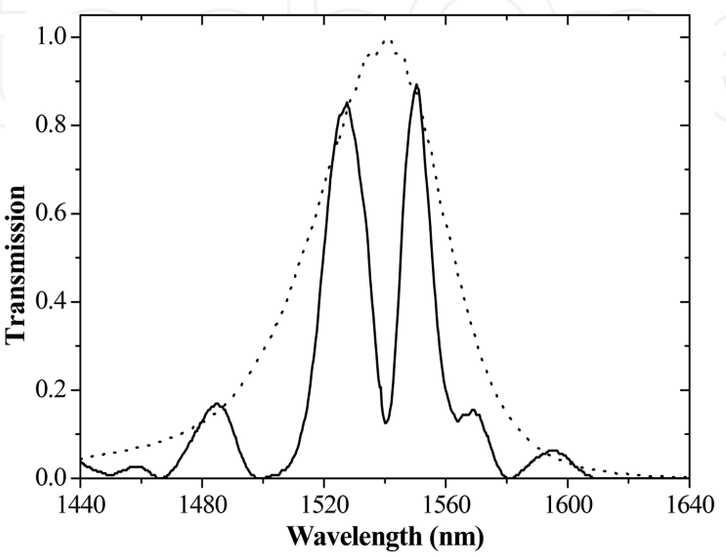


Figure 2.
Normalized transmission spectra of the PCF before (dotted curve) and after (continuous curve) tapering. The taper waist diameter is 28 μm (reprinted with permission from Ref. [19], OSA).

analyzer with a resolution of 0.1 nm. It is possible to note that the transmission of our untapered PCF is basically the output spectrum of the LED used. However, the spectrum of the 28-μm-thick taper exhibits a series of peaks, two of which are higher than the others. For this taper we investigated the shift of the interference peaks caused by longitudinal strain. The PCF was fixed between two displacement mechanical mounts, with the tapered section in the middle. Then the fiber was stretched using the calibrated micrometer screws of the mounts. **Figure 3(a)** shows the normalized spectra, measured at 1540 nm, of the taper, when it has been subjected to 0 (continuous curve), 1100 (dashed curve), and 2200 (dotted curve) με. In this figure we can see shift of the initial spectrum to shorter wavelengths, when the strain is increased. When the strain was removed from the sensor, all the peaks returned to their baselines. At this point, we exchanged the LED for another with peak emission at 1300 nm and repeated the experiments. **Figure 3(b)** shows the normalized spectra, measured at 1300 nm, of the taper, when it also subjected to three applied strains: 0 (continuous curve), 1100 (dashed curve), and 2200 (dotted curve) με. It is possible to see in this figure that the transmission spectrum of the device also exhibits interference peaks near 1300 nm and that such peaks also shift to shorter wavelengths. Note from **Figure 3** that the height of some peaks increases and that of others decreases. All the peaks, however, maintain almost the same shape. The influence of temperature on the peaks was also investigated. The taper subjected to 0 με was exposed to different temperatures between 0 and 180°C. In that range of temperatures the interference peaks did not suffer any shift, but, at higher temperatures, the peaks shifted to longer wavelength. We did not carry out measurements below 0°C because of technical limitations. Hence, a no adiabatic tapered silica PCF with collapsed air holes can be used for temperature-independent strain sensing.

The advantage of the sensor is that one can monitor one or all the peaks. In addition, different wavelengths can be used to interrogate the sensor. **Figure 4** shows the peak shift as a function of the applied strain, when the initial peaks are centered around 1520 and 1250 nm, see **Figure 3(a)** and **(b)**, respectively. It is possible to

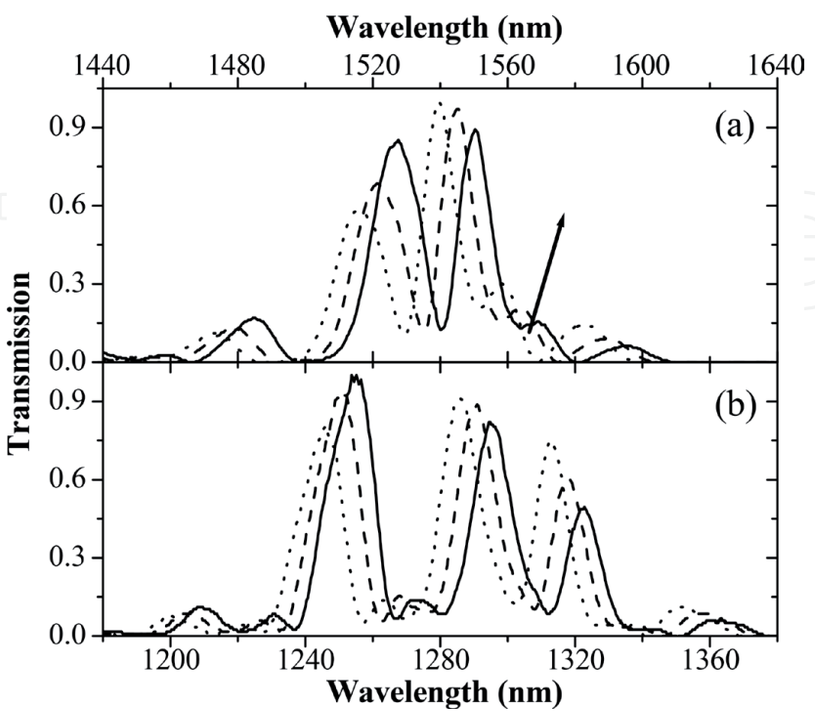


Figure 3.
Normalized transmission spectra of a 28-μm-thick tapered PCF under three applied strains measured at (a) 1550 and (b) 1330 nm. In both figures the continuous curves represent 0 με, the dashed curves 1100 με, and dotted curves 2200 με (reprinted with permission from Ref. [19], OSA).

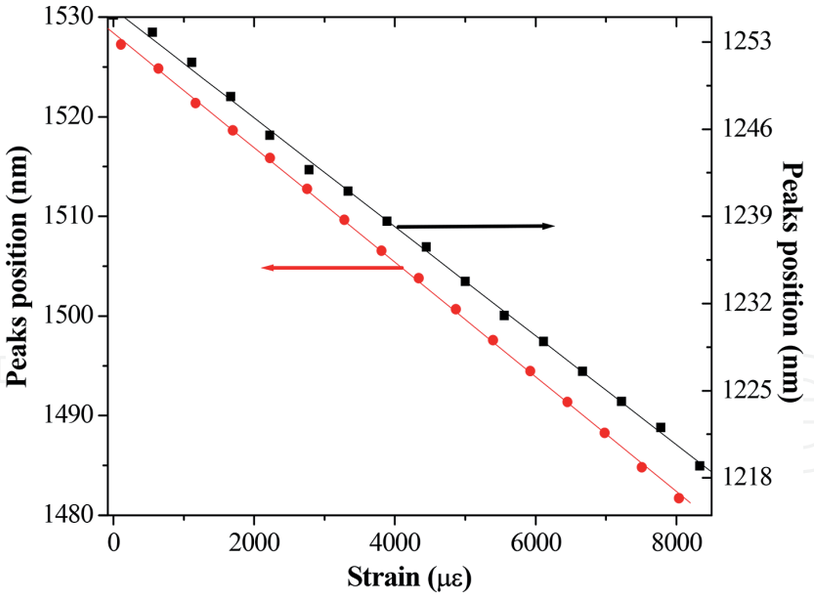


Figure 4.
Typical shift of the peaks as a function of the applied strain (reprinted with permission from Ref. [19], OSA).

note from the figure that the shift of both peaks has a linear behavior and the slope of both lines is basically the same. The observed shift of the other peaks shown in **Figure 3** was also linear, and their slope was similar to that of the peaks shown in **Figure 4**. The experiments were carried out several times. It was observed that in all cases the sensor was reversible in the 0–8000 με range.

It is important to point out that optical fiber interferometric strain sensors are useful devices, because they can provide important information or solutions in a number of applications of practical interest. These sensors, incorporated into civil aircraft and spacecraft structures, smart materials, active devices and components, etc., permit the monitoring of strain-induced changes suffered by such structures, materials, or components. In all these applications, temperature-independent, intrinsic, and wavelength-encoded strain sensors with high resolution are desirable.

4. High-temperature detection

It is known variety of standard fiber-based temperature sensors, for both point and distributed detection. The sensing mechanisms include [21] fluorescence and time decay effects in active materials and doped fibers, remote blackbody radiation, Raman and Brillouin scattering, interferometry, and Bragg or long-period grating technology. The large majority of reported so far fiber temperature sensors have been designed to operate in a range from −20 to 200°C. However, there are some applications in which high-temperature sensing is necessary, for example, for monitoring furnace operation or volcanic events, or in fire alarm systems, etc. [22]. Most of the techniques mentioned in this chapter before are not suitable for high-temperature sensing. Materials traditionally used for fluorescence-based fiber thermometers have an inferior fluorescence intensity emission at temperatures above 600°C [23, 24]. Some interferometric temperature sensors can be designed for measurement of temperatures higher than 1600°C [25, 26]. However, their construction is complicated and a sensing element is external to the fiber. Important advances have been made to fabricate fiber Bragg grating devices for measurement of high temperatures [23], but these devices require a complicated fabrication process or a long and controlled temperature treatment [27–29]. A long-period grating

inscribed with a pulsed CO_2 laser in a PCF [30] or a very small stub of index-guiding PCF fusion spliced between two standard single-mode fibers [31] can be also used for high-temperature measurements. We have proposed a novel high-temperature sensor based on the developed PCF taper with collapsed air holes in the waist [32, 33]. The PCF taper with ρ_w = 31 μm and L_0 = 5 mm (see **Figure 1**) was used for high-temperature measurements. Before the tapering, a few centimeters of the referred PCF were inserted between two standard single-mode fibers (SMF-28) by fusion splicing. Then the PCF was slowly stretched, while a section of length L_0 was heated at a high temperature (at about 1000°C). It is important to point out that the PCF can also be tapered without the need of splicing it with conventional optical fibers. The fabricated taper was placed within a pure silica capillary tube, in order to have the taper straight during experiments (bending affects the sensor response). Then, the whole set was placed into a temperature chamber. To interrogate the device, light was injected from an LED with a peak emission at 1290

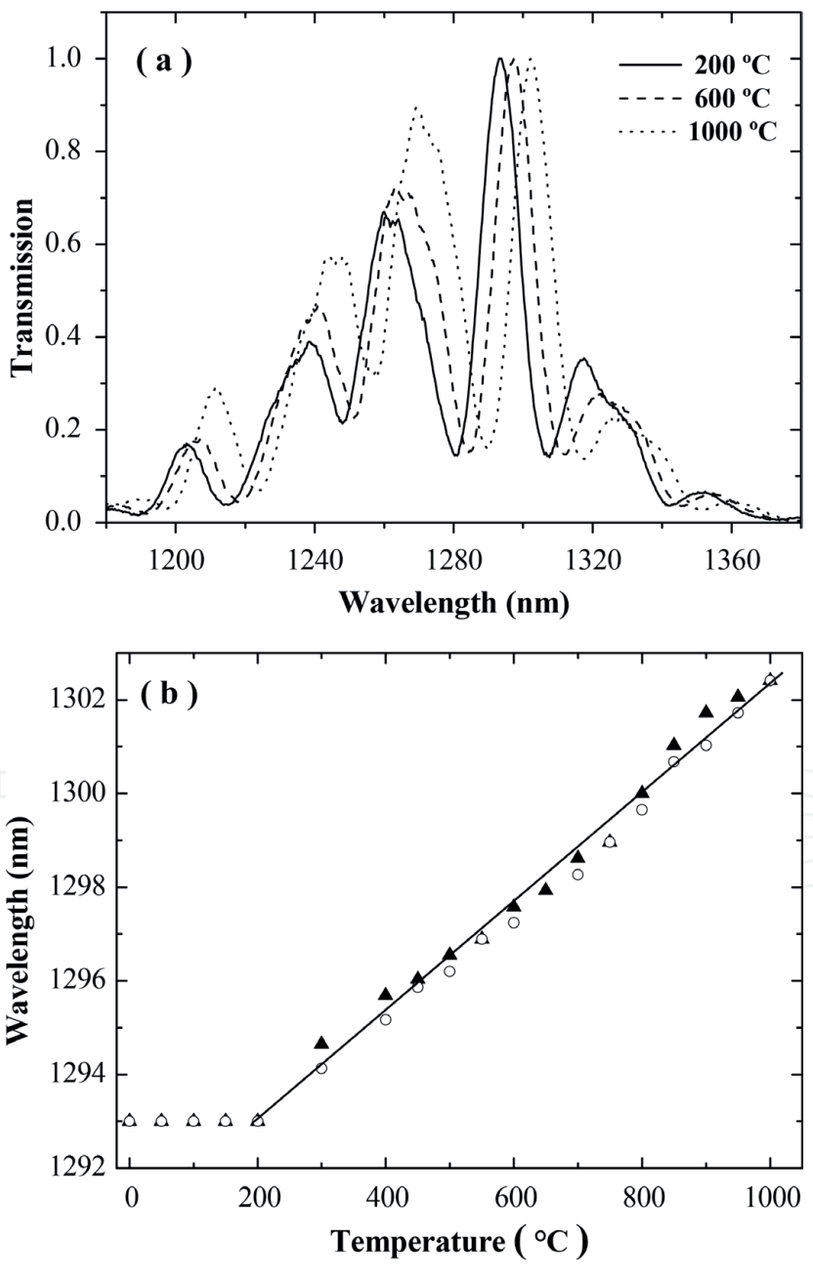


Figure 5.
(a) Normalized transmission spectrum of a taper with ρ_w *= 31 μm and* L_o *= 5 mm, at different temperatures. (b) Position of the highest peak of the spectrum (a) versus temperature. The filled triangles (heating) and the hollow circles (cooling) are experimental values. The solid line is a linear fit to the data in the 200–1000°C range (reprinted with permission from Ref. [32], IEEE).*

and with 80 nm of spectral width. The output spectrum was monitored with an optical spectrum analyzer (OSA) with a resolution of 0.1 nm. We also realized our experiments using an LED, with a center wavelength at 1520 nm and with 40 nm of spectral width. The heating or cooling of the taper in the furnace was conducted in steps of 50°C. In each step of heating or cooling, one waited for about 30 min before collecting any data. With this procedure a homogeneous temperature inside the chamber was ensured. The exhibited around 1300 nm transmission spectra of the referred taper at temperatures of 200°C (solid line), 600°C (dashed line), and 1000°C (dotted line) are shown in **Figure 5(a)**. Measurements for temperatures above 1000°C were not possible for limitations of our furnace. In the plots of **Figure 5(a)**, we can see that the interference peaks shift toward longer wavelengths as the temperature increases. We have also found that the shift of the peaks shown in **Figure 5(a)** using the LED centered at 1290 nm and the shift of the peaks using the LED centered at 1520 nm (is not shown) are similar. This means that the central peak of the LED is not important. One also can see that the peaks are not deformed, when the device is exposed to a temperature higher than 1000°C. This is so, because the fiber was made of pure silica and the taper was fabricated, when the PCF was exposed to a high-temperature flame (of approximately 1000°C). The experiments were repeated several times in a period of 4 weeks, and it was observed the same behavior of the sensor. The position of the highest peak maximum for the spectrum of **Figure 5(a)** versus temperature is shown in **Figure 5(b)**.

One can see that the peaks are insensitive to temperature in the 0–180°C range; but they shift linearly to longer wavelengths in the 200–1000°C range. The slope of the curve in such a range is 12 pm/°C. Deviations from this line were, in our opinion, due to errors in the readings of the furnace temperature and also in the definition of the peak maxima position. The resolution of the sensor can be improved using thinner tapers, which exhibit sharper peaks that are easier to monitor. Unfortunately, thinner tapers are more difficult to work with. Another possibility to improve the sensor resolution is to monitor all the interference peaks and to combine them with a fitting algorithm.

5. Gas detection

To the beginning of our study, several sensors that exploit the direct interaction of evanescent fields of PCF guided modes with the target gas within the holes of unmodified PCFs have been proposed and demonstrated [5, 34–37]. The walls of the PCF air holes can also be covered with thin layers for a selective detection of specific gases [38]. Unfortunately, the filling of the air holes with a target gas is not convenient enough, since it takes a long time. Theoretical and experimental studies have shown that the time for a gas to diffuse into the very small holes of a PCF takes about tens of seconds to several minutes and depends on the fiber length [34]. To the time needed for a gas to diffuse into the holes of a PCF, one has to add the time needed to detect, analyze, and process the signal. Leaving the microscopic holes open in a PCF is also not convenient, since they can be filled with undesirable microparticles or moisture that can block the holes or change an output signal. In some potentially explosive or flammable environment, for example, in hydrogen environments, fast gas detection is necessary, and a rapid response of the sensor is desirable [39]. It is necessary also to remind that even existent this time hydrogen sensors have the response time not fast enough [40, 41]. We proposed the use of developed tapered PCFs, coated with thin layers, which can absorb the sensing gas or chemicals, for faster detection. In the taper waist (see **Figure 1**), the external medium plays the role of cladding, and the solid waist section plays the role of core. Therefore, a thin layer deposited on a waist region will attenuate or absorb the

evanescent fields of different propagating waist modes. As a result, the output pattern of the tapered fiber will be also modified. Thus, the sensing of different gases or any other chemicals is observable. To confirm of the principle, we demonstrated the sensing of hydrogen [42, 43]. Hydrogen is one of the cleanest energy sources. It can be used in many chemical processes and in various fields, for example, as propellant in aerospace rockets, fuel for fuel cells, or engines in automotive devices. However, hydrogen is extremely flammable and can be explosive in air at room temperature and pressure even at concentrations of 4 vol.% and of course at more ones [39]. Therefore, fast detection of hydrogen at low concentrations is necessary. To do so, an ultrathin palladium layer was deposited on a solid section of a tapered PCF. It is well known that a thin palladium (or palladium alloy or composite) film can selectively and reversibly absorb hydrogen [39, 44–51]. When a Pd or Pd-alloy film is exposed to hydrogen, it is converted to PdH. The hydration of the thin film makes the real and imaginary part of the film dielectric constants to decrease [45, 49]. Such changes in the Pd film are possible to monitor with optical methods [39, 44–51].

Using the same fiber, and the same tapering process as in previous sections, a silica PCF taper with waist diameter ρ_w = 28 μm and L_0 = 10 mm was fabricated. An 8-nm-thin film was deposited on the waist of the tapered PCF over a length of 10 mm. The palladium film was deposited in a high-vacuum chamber by thermal evaporation. The sensor was tested (at normal conditions) in a gas chamber, which had an inlet and outlet to allow the hydrogen or the hydrogen/carrier mixture to flow in and out. Nitrogen was used as a carrier gas. The flow of nitrogen and hydrogen was controlled individually with mass flow controllers. The sensor is tested in a transmission measurement setup consisting of a low-power LED with peak emission at 1290 and 80 nm of spectral width and an OSA. The spectra of the device were recorded and analyzed at different concentrations of hydrogen. Before measurements, about 30 cm of the PCF was fusion spliced between two standard single-mode fibers to decrease the sensor cost, and then the tapered section was held straight in a mechanical mount during all the experiments. Results of our experiments are presented in **Figure 6**. The top side plots in **Figure 6** show the spectra that were received, when the sensor was exposed to hydrogen concentrations between 1.2 and 5.6%. Four peaks of the spectra are numbered for convenience. Intensity of the peaks 1–4 as a function of hydrogen concentrations is presented in the bottom side of **Figure 6**. One can see that the intensity of the peaks increases in a nonlinear manner with the increase of the hydrogen concentration. For hydrogen concentrations, more than 6% the sensor exhibited spectra similar to that at 5.6%, which indicated the saturation of the 8-nm-thick palladium film. The reason of increase of the obtained peak intensity is because the index of the thin palladium film decreases, when it is exposed to hydrogen [45, 47, 49]. Such a decrement of the index causes the absorption of the evanescent fields to decrease. The remarkable increment of the peak intensity demonstrates the high sensitivity of the sensor. The sensor response time (the time required for the sensor to reach 90% of transmission change) was approximately 10 s. In **Figure 6** one can see that the intensity changes are more in the peaks or maxima than in the valleys or minima. One can also note that the intensity changes at longer wavelengths, see peaks 3 and 4, are more pronounced than at shorter wavelengths, see peaks 1 and 2. This is due to the fact that the attenuation of the palladium film increases, when the wavelength augments, according to the increase of the evanescent fields [47].

The interferometric hydrogen sensor reported here is more compact, simpler, and also faster than other interferometer-based hydrogen sensors reported in the literature [39, 44–46, 50].

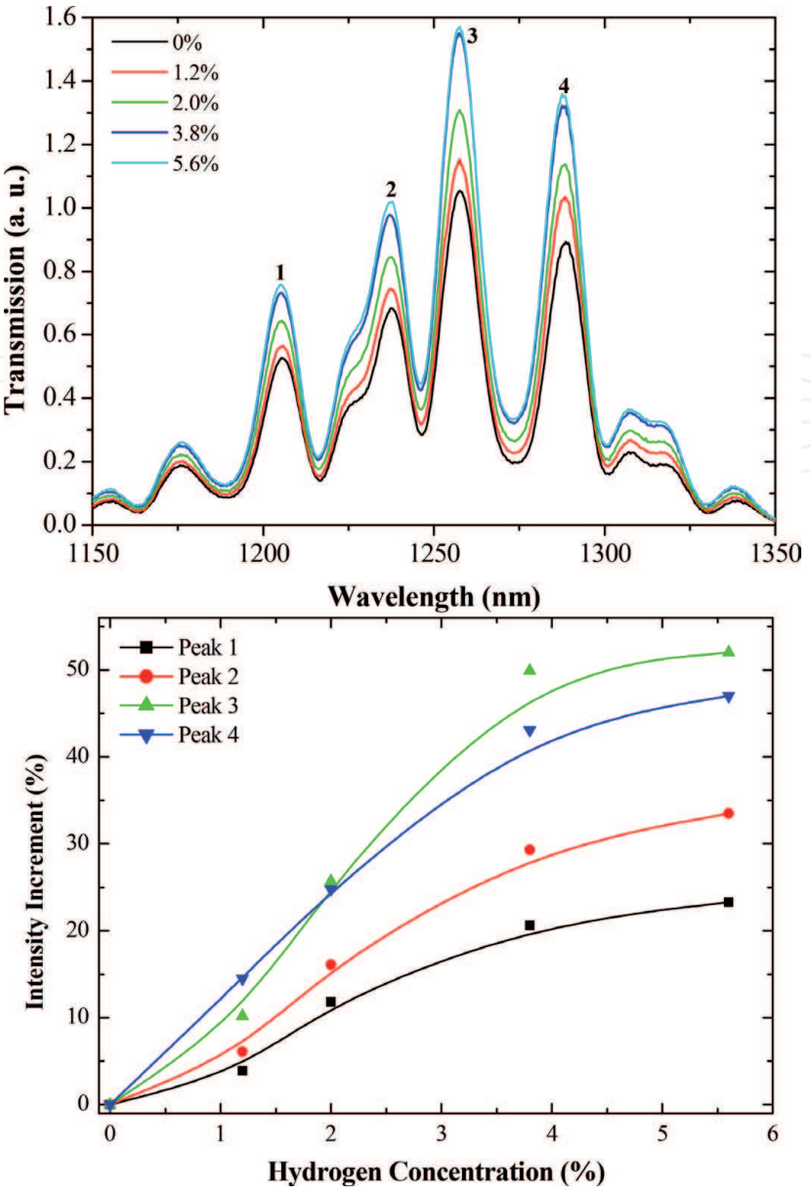


Figure 6.
Transmission spectra of a tapered PCF coated with an 8-nm-thick Pd film at different hydrogen concentrations (top) and relative increment of the peaks 1–4 as a function of hydrogen concentration (bottom). Parameters of the sensor: ρ_w = 28 μm, L_o = 10 mm (reprinted with permission from Ref. [42], OSA).

6. Highly sensitive biosensing

Previous experimental studies of modal interferometers, for the biosensing refractive index (RI) range (1.33–1.34), have informed about sensitivities of 320 nm/RIU for a sensing length of PCF (~3.0 mm) [52] and sensitivities of 1629 nm/RIU for a longer sensing length (~24 mm) [53]. PCF MZMIs based on no adiabatic tapered fibers are attractive for biosensing applications, because they can have a very small sensing length [8, 10]. Unfortunately, PCF MZMI RI sensors for biosensing applications usually can only be used to detect a solution with one analyte and when the RI dependence of an analyte at different concentrations is known. To obtain a specific sensitivity for a chosen analyte in some complex solutions, we coated the sensing surface (tapered PCF) of our RI sensor with a layer of an active biological component (an immobilization method), characterized by having a high affinity with the chosen analyte. The usual immobilization method, for glass substrates, is

through the process of silanization, followed by the covalent bonding of an antigen or antibody [52, 54]. In [52], a detection limit of 10 μg/ml was demonstrated for streptavidin using a modal interferometer based on a short piece of PCF (~3.0 mm) spliced between two standard single-mode fibers, while in [55], a modal interferometer based on a thin-core fiber spliced between two standard single-mode fibers was used, and a detection limit of 1.1 ng/ml was achieved. In this paragraph, we inform about a MZMI based on a no adiabatic tapered special silica PCF acting as a highly sensitive biosensor. We also demonstrated that as a refractometer, it has good sensitivity in the RI range of interest for biological solutions and a record detection limit of 125 pg/ml of a protein concentration as a biosensor [56, 57]. In our experiments we used a homemade large-mode-area photonic crystal fiber. A cross section of the untapered fiber is shown in **Figure 7(a)**. The used fiber has an average hole spacing (pitch) Λ of 5.45 μm, an average hole diameter d of 2.7 μm, and an external diameter of 125 μm. The modal properties of the fiber are explained in [11]. To reduce our sensor cost, we spliced about 30 cm of the PCF between two standard SMF-28 single-mode fibers. The difficulty in splicing the PCF with the used standard SMF is that each one requires different temperatures to reach the needed fusion conditions. A commercial splicing machine, Sumitomo Type-46S, was used in the process. The splicing configuration is shown in **Figure 7(b)**. We used a Vytran GPX3400 glass-processing machine to make the no adiabatic tapering. The tapered fiber for our sensor was fabricated with both transition regions (down taper and up taper) being symmetrical with a length of 5 mm, a waist length of 10 mm, and a waist diameter of 18.1 μm, like the one presented as an example in [58] on a base of a standard fiber. The pulling speed of the fiber holding blocks was kept at a rate of 1 mm/s, while the heat was set at 90 W. We used an LED source with a center wavelength of 1550 nm and an optical spectrum analyzer (OSA), Ando AQ-6315E, which has a resolution of up to 0.05 nm, to make the SM-PC-SM fiber transmission spectrum measurements, as shown in **Figure 8(a)**. To make it easier to measure aqueous solutions with the fiber sensor, a work cell, shown in **Figure 8(b)**, was designed.

The cell was fabricated with a working volume of 50 μl and a cavity length of 13 mm. To test a sensitivity of our device for biosensing RI range, solutions of sodium chloride (NaCl) diluted in distilled water were prepared in the following concentrations, 0.0, 0.2, 0.4, 0.6, 0.8, and 1 M, with corresponding refractive indices at 1550 nm of 1.30864, 1.31104, 1.31339, 1.31569, 1.31794, and 1.32014 [59]. An antigen-antibody test was proposed to evaluate the performance of the device for a biosensor application. We chose the bovine serum albumin (BSA) antigen because of its low cost, ease of handling, availability, and immobilization (covalent binding between the molecule and the transducer surface), which has been widely studied. The immobilization process was conducted like the

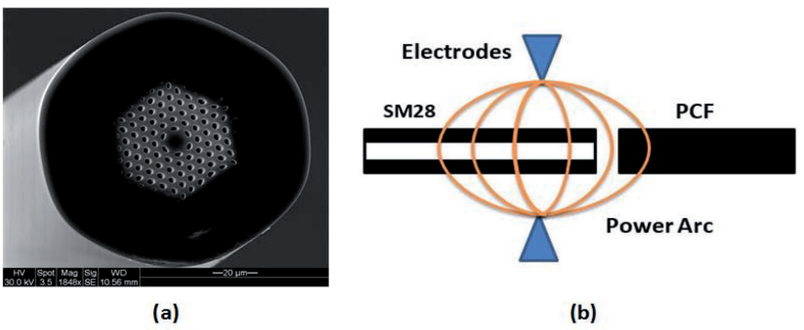


Figure 7.
(a) PCF untapered cross section, (b) SM-PCF splicing configuration (reprinted with permission from Ref. [56], IEEE/OSA).

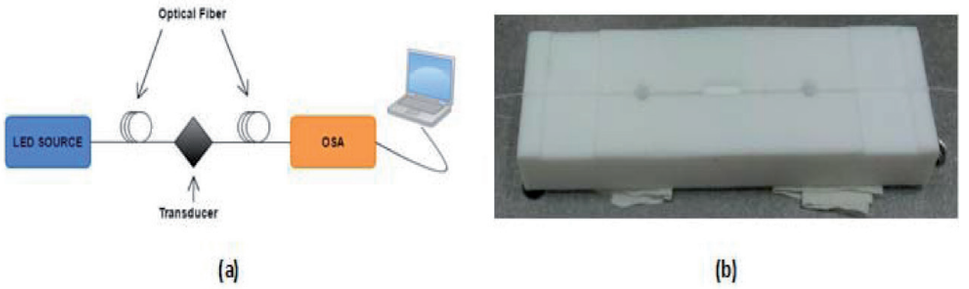


Figure 8.
(a) Experimental setup, (b) work cell (reprinted with permission from Ref. [56], IEEE/OSA).

one presented in [54]. Preliminary, the activation of the taper surface with an aminosilane APTES was made, and then the BSA antigen was covalent coupled to the taper surface. After the antigen-immobilization process, the performance tests were conducted by passing the respective antibody (anti-BSA) diluted in phosphate-buffered saline (PBS) buffer at different concentrations (125, 12.5, 1.25, and 0.125 ng/ml) over the sensitive sensor's surface. All tests were carried out at room temperature, at about 25°C. The protocol used for the tests was as follows. Step 1: Apply tris(hydroxymethyl)aminomethane (TRIS) buffer for 3 min to clean and break previous bonds. Step 2: Remove the TRIS buffer, apply the PBS, and make a measurement of the optical spectrum that corresponds to the baseline. Step 3: Remove the PBS buffer, apply the desired antibody-PBS sample, and take measures for 10 min. Previous experiments have demonstrated that after 6 min of interaction, the variation of the signal can be neglected for practical measurements. For each sample, repeat the protocol. The difference in wavelength between a peak on the baseline and the same peak, measured after 8 min of sample interaction, is the biosensor response, which is directly related to the sample concentration. **Figure 9(a)** shows that as the refractive indices of the NaCl solutions increase, the peaks shift to longer wavelengths. Peaks with similar morphologies were selected for the analysis of the peak shifts. **Figure 9(b)** corresponds to the linear fit built by taking the wavelength of the peak maxima (between 1538 and 1548 nm) and correlating them with the respective RI. A sensitivity of 722.3 nm/RIU was achieved (with a linearity of 0.9965), which can be compared with other sensors reported. **Figure 10** shows the results of the biosensor application, where the magnitude of the response is directly proportional to the anti-BSA concentration.

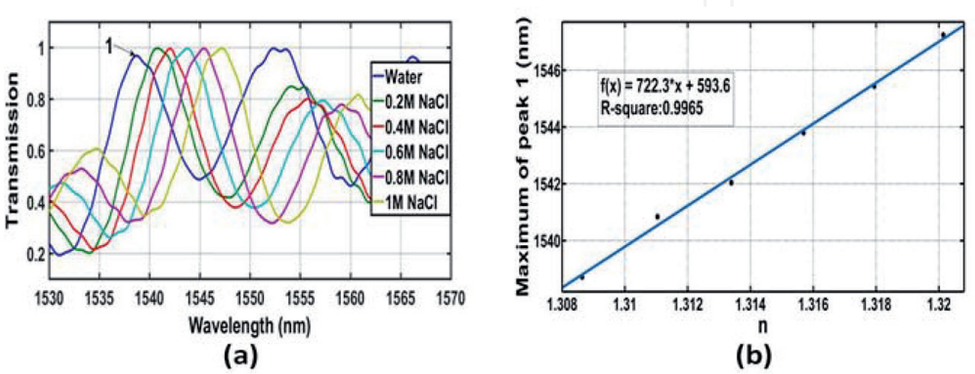


Figure 9.
(a) Transmission spectra of the sensor at different concentrations of NaCl, (b) linear fit of the sensor response for concentrations of NaCl with RI between 1.30864 and 1.32014 (reprinted with permission from Ref. [56], IEEE/OSA).

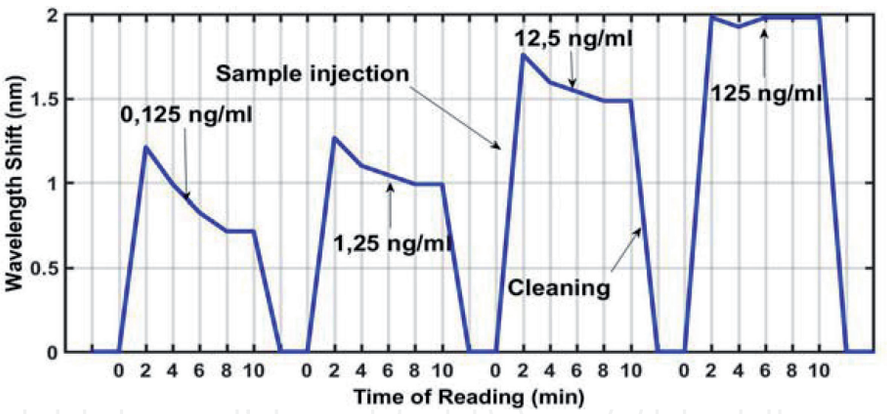


Figure 10.
Sensor response for concentrations of anti-BSA between 0.125 and 125 ng/ml (reprinted with permission from Ref. [56], IEEE/OSA).

We can see in **Figure 10** that the sensor can take measurements of concentrations as low as 125 pg/ml; this means that our detection limit is lower than the one reported in [58]. Another fact to highlight is that our sensor is capable to detect a specific protein inside a complex sample (with different proteins diluted) that is not possible for the sensor proposed in [58]. The increased sensitivity in our case is possible, when compared with that in [58], because in [58] the detection of protein concentrations was done by reading a change in the refractive index of the bulk solution; therefore, higher concentrations were needed to produce a change big enough to be detected by the sensor. In our case, the antigen of the target molecule was immobilized onto the transducer surface, making it possible to detect the antigen-antibody interaction with higher sensitivity. The changes in refractive index near the surface are mostly affected by the coupling of the specific protein and not by other proteins in the sample. In addition, the area near the surface of the fiber has exponentially higher sensitivity than areas that are farther away. The developed sensor also has a lower detection limit when compared with those reported in [52, 55], with detection limits of 10 and 1.1 ng/ml, respectively, outperforming the former in three orders of magnitude and the latter in one order of magnitude. It is also necessary to point out that the estimated maximum resolution of our sensor was found to be around 1×10^{-2} ng/ml, considering that the resolution of the spectrum analyzer used was 0.05 nm. The higher resolution of our measurements is possible at using an OSA with higher resolution. More precise localization of interference fringes by performing a Fourier transformation will be also helpful [60]. As can be also seen in **Figure 10**, we did not have any saturation in a sensor response for concentrations of anti-BSA between 0.125 and 125 ng/ml, although the spectral shift had highly nonlinear dependence on the anti-BSA concentration. Comparing with **Figure 10**, where we had a linear dependence of our sensor response and did not have any chemical binding between NaCl solutions and the taper surface, one can conclude that the antibody-antigen binding process has a great impact on our sensor response. A definition of the impact requires further investigations.

7. Conclusions

In this chapter, a special homemade quasi-single-mode PCF was used for fabrication of no adiabatic tapered fibers with a solid waist. The fabrication of tapers is simple and takes only few minutes. It is also possible to control the process of tapering at all times. It has been found that in PCF tapers with waist diameters small

enough (thinner than 33 μm), the air holes of a PCF cladding were collapsed. A waist of such tapers consists of a solid multimode fiber supporting multiple modes. The interference between such modes gives series of peaks in an output spectrum pattern. The peaks are sensitive to a medium that surrounds the taper and also to the length of the waist, since the propagation constants of the interfering modes depend on them. Any changes in a surrounding medium or in the length of the taper are visualized as a shift of peaks in the output spectrum pattern. The tapers were used for fabrication of very sensitive interferometric devices with selective transmission for temperature-insensitive detection (in the 0–180°C range) of microstrain, for sensing of high temperature in the 200–1000°C range, and for fast detection of hydrogen concentrations between 1.2 and 5.6 vol.%. Moreover, the developed interferometers can be used for detection of interaction between a BSA antigen and an anti-BSA antibody with a record detection limit of 125 pg/ml of antibody concentration. The parameters that are necessary to measure by using the interferometers are transformed into the shift of peaks in the output spectrum pattern. It is not difficult by using an optical spectrum analyzer to monitor the shift. Detection is fast and takes approximately 10 s. It is necessary also to note that the output spectrum patterns are stable and immune to possible fluctuations of a light source power.

Acknowledgements

The authors of the chapter would like to thank their colleagues and co-authors of joint publications Monzon-Hernandez D, Kir'yanov AV, Calixto S, Sotsky AB, Sotskaya LI, Badenes G, Betancur-Ochoa JE, and Montagut-Ferizzola YJ for long-term and productive scientific cooperation.

Author details

Vladimir (or Uladzimir) P. Minkovich[1*], Joel Villatoro[2,3] and Pavel V. Minkovich[4]

1 Division of Photonics, Centro de Investigaciones en Optica, Leon, GTO, Mexico

2 Department of Communications Engineering, University of the Basque Country, Bilbao, Spain

3 Ikerbasque-Basque Foundation for Science, Bilbao, Spain

4 Mogilev State Medical College, Mogilev, Belarus

*Address all correspondence to: vladimir@cio.mx

IntechOpen

© 2018 The Author(s). Licensee IntechOpen. This chapter is distributed under the terms of the Creative Commons Attribution License (http://creativecommons.org/licenses/by/3.0), which permits unrestricted use, distribution, and reproduction in any medium, provided the original work is properly cited. CC BY

References

[1] Knight JC, Birks TA, Russell PSJ, Atkin DM. All-silica single-mode optical fiber with photonic crystal cladding. Optics Letters. 1996;**21**:1547-1549. DOI: 10.1364/OL.21.001547

[2] Russell P. Photonic crystal fibers. Science. 2003;**299**:358-362. DOI: 10.1126/science.1079280

[3] Bjarklev A, Broeng J, Bjarklev AS. Photonic Crystal Fibres. Boston, MA: Kluver Academic Publishers; 2003. 298 p. ISBN: 1-4020-7610-X

[4] Russell PSJ. Photonic crystal fibers. Journal of Lightwave Technology. 2006;**24**:4729-4749. DOI: 10.1109/JLT.2006.885258

[5] Monro TM, Belardi W, Furusawa K, Baggett JC, Broderick NGR, Richardson DJ. Sensing with microstructured optical fibers. Measurement Science and Technology. 2001;**12**:854-858. DOI: 10.1088/0957-0233/12/7/318

[6] Konorov SO, Zheltikov A, Scalora M. Photonic-crystal fiber as a multifunctional optical sensor and sample collector. Optics Express. 2005;**13**:3454-3459. DOI: 10.1364/OPEX.13.003454

[7] Cubillas AM, Unterkofler S, Euser TG, Etzold BJM, Jones AC, Sadler PJ, et al. Photonic crystal fibres for chemical sensing and photochemistry. Chemical Society Reviews. 2013;**42**:8629-8648. DOI: 10.1039/C3CS60128E

[8] Minkovich VP, Villatoro J, Monzón-Hernández D, Calixto S, Sotsky AB, Sotskaya LI. Holey fiber tapers with resonance transmission for high-resolution refractive index sensing. Optics Express. 2005;**13**:7609-7614. DOI: 10.1364/OPEX.13.007609

[9] Minkovich VP, Monzón-Hernández D, Villatoro J, Sotsky AB, Sotskaya LI. Modeling of holey fiber tapers with selective transmission for sensor application. Journal of Lightwave Technology. 2006;**24**:4319-4326. DOI: 10.1109/JLT.2006.884207

[10] Villatoro J, Minkovich VP, Monzon-Hernandez D. Compact modal interferometer built with tapered microstructured optical fiber. IEEE Photonics Technology Letters. 2006;**18**:1258-1260. DOI: 10.1109/LPT.2006.875520

[11] Minkovich VP, Kir'yanov AV, Sotsky AB, Sotskaya LI. Large-mode-area holey fibers with a few air channels in cladding: Modeling and experimental investigation of the modal properties. Journal of the Optical Society of America B: Optical Physics. 2004;**21**:1161-1169. DOI: 10.1364/JOSAB.21.001161

[12] Kersey AD, Davis MA, Patrick HJ, LeBlanc M, Koo KP, Askins CG, et al. Fiber grating sensors. Journal of Lightwave Technology. 1997;**15**:1442-1463. DOI: 10.1109/50.618377

[13] Ohno H, Naruse H, Kihara M, Shimada A. Industrial applications of the BOTDR optical strain sensors. Optical Fiber Technology. 2001;**7**:45-64. DOI: 10.1006/ofte.2000.0344

[14] Villatoro J, Finazzi V, Minkovich VP, Pruneri V, Badenes G. Temperature-insensitive photonic crystal fiber interferometer for absolute strain sensing. Applied Physics Letters. 2007;**91**:AD091109. DOI: 10.1063/1.2775326

[15] Zou L, Bao X, Afshar S, Chen L. Dependence of the Brillouin frequency shift on strain and temperature in a photonic crystal fiber. Optics Letters. 2004;**29**:1485-1487. DOI: 10.1364/OL.29.001485

[16] Zhu Y, Shum P, Bay HW, Yan M, Yu X, Hu J, et al. Strain-insensitive and high-temperature long-period gratings inscribed in photonic crystal fiber. Optics Letters. 2005;**30**:367-369. DOI: 10.1364/OL.30.000367

[17] Martelli C, Canning J, Groothoff N, Lyytikainen K. Strain and temperature characterization of photonic crystal fiber Bragg grating. Optics Letters. 2005;**30**:1785-1787. DOI: 10.1364/OL.30.001785

[18] Frazão O, Carvalho JP, Ferreira LA, Araujo FM, Santos JL. Discrimination of strain and temperature using Bragg gratings in microstructured and standard optical fibers. Measurement Science and Technology. 2005;**16**:2109-2113. DOI: 10.1088/0957-0233/16/10/028

[19] Villatoro J, Minkovich VP, Monzon-Hernandez D. Temperature-independent strain sensor made of tapered holey optical fiber. Optics Letters. 2006;**31**:305-307. DOI: 10.1364/OL.31.000305

[20] Minkovich VP, Villatoro J, Monzon-Hernandez D. Method for Monitoring Strain using Tapered Microstructured Optical Fiber. European Patent No. EP1962120B1; 2013

[21] Lopez-Higuera JM, editor. Handbook of Optical Fibre Sensing Technology. Chichester: Wiley; 2002. 795 p. ISBN: 0-471-82053-9

[22] Brambilla G, Kee HH, Prunery V, Newson TP. Optical fibre sensors for earth science: From the basic concepts to optimizing glass composition for high temperature applications. Optics and Lasers in Engineering. 2002;**37**:215-232. DOI: S0143-8166(01)00096-3

[23] Shen YH, Pal S, Mandal J, Sun T, Grattan KTV, Wade SA, et al. Investigation of the photosensitivity, temperature sustainability and fluorescence characteristics of several Er-doped photosensitive fibers. Optics Communication. 2004;**237**:301-308. DOI: 10.1016/j.opticom.2004.04.004

[24] Shen Y, Zhao W, Sun T, Grattan KTV. Characterization of an optical fiber thermometer using Tm^{3+}:YAG crystal, based on the fluorescent lifetime approach. Sensors and Actuators, A: Physical. 2003;**109**:53-59. DOI: 10.1016/j.sna.2003.09.006

[25] Zhu Y, Huang Z, Shen F, Wang A. Sapphire-fiber-based white-light interferometric sensor for high-temperature measurements. Optics Letters. 2005;**30**:711-713. DOI: 10.1364/OL.30.000711

[26] Xiao H, Deng J, Pickrell G, May RG, Wang A. Single-crystal sapphire fiber-based strain sensor for high-temperature applications. Journal of Lightwave Technology. 2003;**21**:2276-2283. DOI: 10.1109/JLT.2003.816882

[27] Lowder TL, Smith KH, Ipson BI, Hawkins AR, Selfridge RH, Schultz SM. High-temperature sensing using relief fiber Bragg gratings. IEEE Photonics Technology Letters. 2005;**17**:1926-1968. DOI: 10.1109/LPT.2005.852646

[28] Forkine M. Thermal stability of chemical composition gratings in fluorine-germanium-doped silica fibers. Optics Letters. 2002;**27**:1016-1018. DOI: 10.1364/OL.27.001016

[29] Trpkovsky S, Kitcher DJ, Baxter GW, Collins SF, Wade SA. High-temperature-resistant chemical composition Bragg gratings in Er^{3+}-doped optical fiber. Optics Letters. 2005;**30**:607-609. DOI: 10.1364/OL.30.000607

[30] Zhu Y, Shum P, Bay HW, Yan M, Yu X, Hu J, et al. Strain-insensitive and high-temperature long-period grating inscribed in photonic crystal fiber. Optics Letters. 2005;**30**:367-369. DOI: 10.1364/OL.30.000367

[31] Coviello G, Finazzi V, Villatoro J, Pruneri V. Thermally stabilized PCF-based sensor for temperature measurements up to 1000°C. Optics Express. 2009;**17**:21531-21559. DOI: 10.1364/OE.17.021551

[32] Monzon-Hernandez D, Minkovich VP, Villatoro J. High-temperature sensing with tapers made of microstructured optical fibers. IEEE Photonics Technology Letters. 2006;**18**:511-513. DOI: 10.1109/LPT.2005.863173

[33] Minkovich U. Special Photonic Crystal Fibers. Saarbrücken: Lambert Academic Publishing; 2011. 74 p. ISBN: 978-3-8465-3622-3

[34] Hoo YL, Jin W, Shi C, Ho HL, Wang DN, Ruan SC. Design and modeling of a photonic crystal fiber gas sensor. Applied Optics. 2003;**42**:3509-3515. DOI: 10.1364/AO.42.003509

[35] Ritari T, Tuominen J, Ludvigsen H, Petersen JC, Sorensen T, Hansen TP, et al. Gas sensing using air-guiding photonic bandgap fibers. Optics Express. 2004;**12**:4080-4087. DOI: 10.1364/OPEX.12.004080

[36] Pickrell G, Peng W, Wang A. Random-hole optical fiber evanescent-wave gas sensing. Optics Letters. 2004;**29**:1476-1478. DOI: 10.1364/OL.29.001476

[37] Fini JM. Microstructure fibres for optical sensing in gases and liquids. Measurement Science and Technology. 2004;**15**:1120-1128. DOI: 10.1088/0957-0233/15/6/011

[38] Matejec V, Mrazek J, Hayer M, Kask I, Peterka P, Kanka J, et al. Microstructure fibers for gas detection. Materials Science and Engineering: C. 2006;**26**:317-321. DOI: 10.1016/J.msec.2005.10.43

[39] Silva SF, Coelho L, Frazão O, Santos JL, Malcata FX. A review of palladium-based fiber-optic sensors for molecular hydrogen detection. IEEE Sensors Journal. 2012;**12**:93-102. DOI: 10.1109/JSEN.2011.2138130

[40] Huang P-C, Chen Y-P, Zhang G, Song H, Liu Y. Note: Durability analysis of optical fiber hydrogen sensor based on Pd-Y alloy film. The Review of Scientific Instruments. 2016;**87**:026104. DOI: 10.1063/1.4941749

[41] Zhang Y-N, Wu Q, Peng H, Zhao Y. Photonic crystal fiber modal interferometer with Pd/WO_3 coating for real-time monitoring of dissolved hydrogen concentration in transformer oil. The Review of Scientific Instruments. 2016;**87**:125002. DOI: 10.1063/1.4971321

[42] Minkovich VP, Monzon-Hernandez D, Villatoro J, Badenes G. Microstructured optical fiber coated with thin films for gas and chemical sensing. Optics Express. 2006;**14**:8413-8418. DOI: 10.1364/OE.14.008413

[43] Minkovich VP, Villatoro J, Sotsky AB. Tapered photonic crystal fibers coated with ultra-thin films for highly sensitive bio-chemical sensing. In: Proceedings of the European Optical Society Biennal Meeting (EOSAM); 8-12 October 2018. Netherlands: Delft; 2018. pp. 1-2

[44] Butler MA. Optical fiber hydrogen sensor. Applied Physics Letters. 1984;**45**:1007-1009. DOI: 10.1063/1.95060

[45] Bearzotti A, Caliendo C, Verona E, D'Amico A. Integrated optic sensor for the detection of H_2 concentrations. Sensors and Actuators B: Chemical. 1992;**7**:685-688. DOI: 10.1016/0925-4005(92)80386-C

[46] Wang C, Mandelis A, Garcia JA. Detectivity comparison between thin-film Pd/PVDF photopyroelectric interferometric and optical reflectance

hydrogen sensors. The Review of Scientific Instruments. 1999;**70**: 4370-4376. DOI: 10.1063/1.1150082

[47] Villatoro J, Diez A, Cruz JL, Andres MV. In-line highly sensitive hydrogen sensors based on palladium-coated single-mode tapered fibers. IEEE Sensors Journal. 2003;**3**:533-537. DOI: 10.1109/JSEN.2003.815789

[48] Ortigosa-Blanch A, Diez A, Gonzáles-Segura A, Cruz JL, Andres MV. Wavelength-codified fiber laser hydrogen detector. Applied Physics Letters. 2005;**87**:201104. DOI: 10.1063/1.2130531

[49] Zhao Z, Carpenter MA, Xia H, Welch D. All-optical hydrogen sensor based on a high alloy content palladium thin film. Sensors and Actuators B: Chemical. 2006;**113**:532-538. DOI: 10.1016/j.snb.2005.03.070

[50] Lin H, Gao T, Fantini J, Sailor MJ. A porous silicon-palladium composite film for optical interferometric sensing of hydrogen. Langmuir. 2004;**20**: 5104-5108. DOI: 10.1021/la049741u

[51] Xu T, Zach MP, Xiao ZL, Rosenmann D, Welp U, Kwok WK, et al. Self-assembled monolayer-enhanced hydrogen sensing with ultrathin palladium films. Applied Physics Letters. 2005;**86**:203104. DOI: 10.1063/1.1929075

[52] Juan Hu DJ, Lim JL, Park MK, Kao LT-H, Wang Y, Wei H, et al. Photonic crystal fiber-based interferometric biosensor for streptavidin and biotin detection. IEEE Journal of Selected Topics in Quantum Electronics. 2012;**18**:1293-1297. DOI: 10.1109/JSTQE.2011.2169492

[53] Li C, Qiu S-J, Chen Y, Xu F, Lu Y-Q. Ultra-sensitive refractive index sensor with slightly tapered photonic crystal fiber. IEEE Photonics Technology Letters. 2012;**24**:1771-1774. DOI: 10.1109/LPT.2012.2214379

[54] Nagel T, Ehrentreich-Forster E, Singh M, Shmitt K, Brandenburg A, Berka A, et al. Direct detection of tuberculosis infection in blood serum using three optical label-free approaches. Sensors and Actuators B: Chemical. 2008;**129**:934-940. DOI: 10.1016/j.snb.2007.10.009

[55] Yu W, Lang T, Bian J, Kong W. Label-free fiber optic biosensor based on thin-core modal interferometer. Sensors and Actuators B: Chemical. 2016;**228**:322-329. DOI: 10.1016/j.snb.2016.01.029

[56] Betancur-Ochoa JE, Minkovich VP, Montagut-Ferizzola YJ. Special photonic crystal modal interferometer for highly sensitive biosensing. Journal of Lightwave Technology. 2017;**35**:4747-4751. DOI: 10.1109/JLT.2017.2761738

[57] Betancur-Ochoa JE, Minkovich VP, Montagut-Ferizzola YJ, Minkovich PV. Highly sensitive biosensing based on a photonic crystal fiber modal interferometer. In: Proceedings of OSA International Conference on Optical Fiber Sensors (OFS 26); 24-28 September 2018; Lausanne: OSA; 2018. p. WF58(1-4)

[58] Yadav TK, Narayasnaswamy R, Abu Bacar MH, Mustafa Kamil Y, Mahdi MA. Single-mode tapered fiber-optic interferometric based refractive index sensor and its application to protein sensing. Optics Express. 2014;**22**:22802-22807. DOI: 10.1364/OE.22.022802

[59] Li X, Liu L, Zhao J, Tan J. Optical properties of sodium chloride solution within spectral range from 300 to 2500 nm at room temperature. Applied Spectroscopy. 2015;**69**:635-640. DOI: 10.1366/14-07769R

[60] Jiang Y. Fourier transform white-light interferometry for the measurement of fiber-optic extrinsic Fabry-Perot interferometric sensors. IEEE Photonics Technology Letters. 2008;**20**:75-77. DOI: 10.1109/LPT.2007.912567